Materials Characterization 132 (2017) 205–214

Contents lists available at ScienceDirect

Materials Characterization

journal homepage: www.elsevier.com/locate/matchar

Influence of mode of plastic straining on the microstructure of Ni and Ti deformed through rolling and torsion

C.N. Athreya[a,*], G. Kapoor[b], J. Gubicza[b], V. Subramanya Sarma[a]

[a] Department of Metallurgical and Materials Engineering, Indian Institute of Technology Madras, Chennai 600036, India
[b] Department of Materials Physics, ELTE Eötvös Loránd University, Pázmány Péter sétány 1/A., Budapest H-1117, Hungary

ARTICLE INFO

Keywords:
Nickel
Titanium
Rolling
Torsion
Dislocations
Twinning

ABSTRACT

The influence of the mode of deformation (rolling and torsion) on the microstructures in Ni and Ti was studied. The microstructure of samples deformed to the same von Mises equivalent strains were characterized by electron backscatter diffraction (EBSD) and X-ray line profile analysis (XLPA). The maximum equivalent strains for Ni and Ti were 2.65 and 0.5, respectively. It was found that despite the same equivalent strains, significant differences were found in the microstructures deformed by rolling or torsion. For instance, the Ni sample rolled to the equivalent strain of 2.65 has larger grain size with less distorted grain interiors than in the specimen torsion tested to the same strain. This difference resulted in a lower stored energy in the rolled sample. The difference in stored energy and lattice strain between rolled and torsion deformed samples is attributed to differences in slip activity in each mode of deformation. In the case of Ti, the initial texture resulted in different contributions of $< c >$ / $< c + a >$ dislocation slip and twinning to plastic deformation during rolling and torsion. Due to the higher twinning activity in the Ti specimen rolled to the strain of 0.5, the fraction of $< c >$ / $< c + a >$ dislocations is smaller than in the torsion tested sample. Despite the different microstructures, the stored energies in the two Ti materials do not differ significantly, as the lower fraction of $< c >$ / $< c + a >$ dislocations in the rolled sample is compensated by their less clustered arrangement.

1. Introduction

The microstructure and properties of metallic materials can be tailored through thermomechanical processing (TMP), involving sequences of cold/hot deformation (e.g., through rolling, forging and drawing) and annealing cycles [1]. During TMP, static recrystallization (SRX) and dynamic recrystallization (DRX) are important phenomena that affect the microstructure development. The SRX and DRX depend not only on the overall stored energy but also on the spatial distribution of defects. The heterogeneity in the deformed microstructure is an important factor that influences the recrystallization kinetics as well as the resulting microstructure and texture [1,2]. During TMP, materials undergo deformation under different states of stress depending on the deformation mode, e.g., forging, rolling, extrusion etc. In view of this, for analysing the recrystallization behaviour of materials it is important to understand the influence of the deformation mode on the strained microstructure. Surprisingly, there are very few studies in the literature that analysed the influence of the deformation mode on the microstructure and its effect on SRX/DRX behaviour [3–7]. In our recent study on Ni [8], we observed that for a given equivalent von Mises strain (ε_{VM} = 1.6 and 2.65), deformation by torsion had resulted in a larger fraction of high angle grain boundaries (HAGBs) and a higher density of potential recrystallization nuclei when compared to samples subjected to rolling. The above differences were attributed to the dependence of the slip system activity on the stress state. The SRX kinetics of torsion deformed Ni samples was significantly faster and the grain sizes were smaller when compared to rolled samples [9].

α-Ti is a low symmetry hexagonal close-packed (HCP) structure with significant anisotropy that undergoes deformation through dislocation slip and twinning [10–12]. Ti samples deformed through hot rolling under different strain paths has been shown to exhibit different textures [10] and stored energy values [13]. The slip activity and propensity of twinning during tension and compression are shown to be strongly dependent on orientation [14,15]. The bulk mechanical properties of Ti are orientation dependent and it depends on the basal/near-basal orientation [16]. The microstructure and texture of deformed and annealed Ti depends on the rolling mode, i.e., unidirectional rolling and multistep cross rolling [17]. Ti samples with different initial texture after compression to same strain exhibited different recrystallization rates during annealing [18]. It can therefore be expected

* Corresponding author.
E-mail address: cnathreya@gmail.com (C.N. Athreya).

http://dx.doi.org/10.1016/j.matchar.2017.08.018
Received 3 August 2017; Received in revised form 11 August 2017; Accepted 21 August 2017
Available online 23 August 2017

that the stress state will have a significant effect on the microstructural evolution in Ti. To the best of our knowledge, there is no systematic study in the literature on the effect of the straining mode on the deformed microstructure in HCP metals from the perspective of recrystallization.

In this study, the influence of the mode of deformation (rolling and torsion) on the deformation microstructure from the perspective of recrystallization is analysed in Ni and Ti samples using electron backscattering diffraction (EBSD) in scanning electron microscope (SEM) and X-ray line profile analysis (XLPA). Ni and commercial purity (CP) Ti (referred to as Ti hereafter) are selected as model materials as they represent a medium stacking fault energy face-centered cubic (FCC) material (which undergoes deformation through slip only at ambient temperature), and an HCP material (which undergoes deformation through both slip and twinning at ambient temperature), respectively. In our previous study on Ni, the samples were deformed to large strains (ε_{VM} = 1.6 and 2.65) and the microstructural heterogeneities were analysed using EBSD [8]. In the present study, we report microstructural analysis on Ni samples deformed through rolling and torsion to equivalent strains of ε_{VM} = 0.5, 2.65 and Ti samples deformed through rolling and torsion to equivalent strains of ε_{VM} = 0.33, 0.5, respectively. In addition, the energy stored in the microstructure is calculated. The microstructures and stored energies obtained for the samples deformed by rolling and torsion are compared.

2. Material and Methods

Ni and Ti samples for torsion and rolling deformation were machined out of extruded rods with the diameters of 15 mm (shown in Fig. 1). Torsion test details and specimen dimensions are given in [19]. Ni samples were deformed through free end torsion for 2 and 9.6 turns.

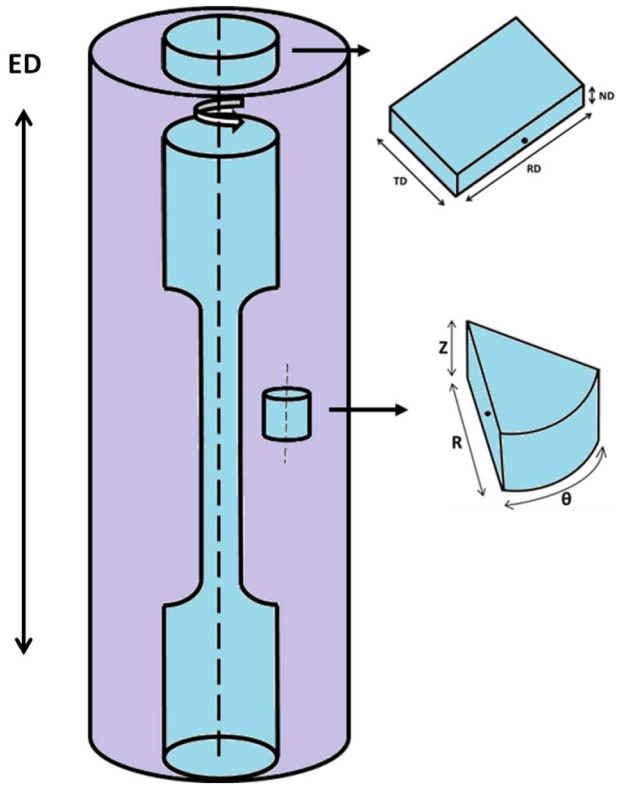

Fig. 1. Schematic of rolling and torsion test sample obtained from annealed extruded Ni and Ti rod. ED: extrusion direction of rod, RD: rolling direction, ND: normal direction and TD: transverse direction of rolling sample, Z: axial direction, R: radial direction and θ: tangential direction of torsion test sample. The dots indicate the sections on which EBSD was performed.

Ti samples were deformed through free end torsion for 2 turns at which sample failed. In the case of the torsion tested samples, the strain varies along the specimen radius and hence sections corresponding to ε_{VM} values introduced through rolling were studied. The von Mises equivalent strain along the radius of the torsion tested samples can be calculated as:

$$\varepsilon_{VM} = \frac{\theta r}{\sqrt{3}\, l} \tag{1}$$

where θ, l and r are the angle of rotation, the height of the cylindrical specimen (l = 38 mm in this case) and the distance from the sample center, respectively.

Ni samples were rolled to the thickness reductions of 35% and 90% which correspond to ε_{VM} of 0.5 and 2.65, respectively, as calculated from the following formula:

$$\varepsilon_{VM} = \frac{2}{\sqrt{3}}\, ln \frac{1}{1-t} \tag{2}$$

where t is the thickness reduction. The Ti samples were rolled to the thickness reduction levels of 25% and 35% which correspond to ε_{VM} of 0.33 and 0.5, respectively. The rolling was performed with 5% reduction per pass for both and Ni and Ti samples.

The microstructural characterization of the deformed samples was carried out by XLPA and EBSD. For XLPA, X-ray diffraction patterns were measured by a high-resolution rotating anode diffractometer (Rigaku) with CuKα_1 radiation (wavelength: λ = 0.15406 nm). The Debye–Scherrer diffraction rings were detected by two dimensional imaging plates and the line profiles were determined as the intensity distributions perpendicular to the rings. The evaluation of the patterns was carried out by the Convolutional Multiple Whole Profile (CMWP) fitting method [20]. In this procedure, the experimental diffraction pattern is fitted by the sum of a background spline and the convolution of the theoretical line profiles related to crystallite size and dislocations. The theoretical line profile functions used in this fitting procedure were based on a model of the microstructure where the crystallites (or coherently scattering domains) have spherical shape and a log-normal size distribution. The following parameters of the microstructure were determined by the CMWP fitting procedure: the mean crystallite size ($< x >$), the average dislocation density (ρ) and the dislocation arrangement parameter M. The dimensionless parameter M is calculated as $R_e\rho^{1/2}$ where R_e is the effective outer cut-off radius of dislocations. The value of M reflects the arrangement of the dislocations. Thus, a smaller value of M relates to a more shielded strain field of dislocations and the arrangement of dislocations into low energy configurations, such as low angle grain boundaries (LAGBs) or dipoles, yields a consequent decrease in M. The mean crystallite size ($< x >$) was calculated as $< x > = m \cdot \exp.(0.5\,\sigma^2)$, where m is the median and σ^2 is the log-normal variance of the crystallite size distribution.

For EBSD, samples were prepared through metallographic polishing with final stage of polishing being done with colloidal silica (particle size: 0.05 μm). In the case of Ti, a second step of polishing was also applied using a mixture of 70% colloidal silica (particle size: 0.05 μm) and 30% hydrogen peroxide. The analysis of the microstructure was carried out on the central region of the RD-ND plane (see Fig. 1) for the rolled samples. In the case of the torsion-tested samples, the microstructure was studied at the locations of the Z-R section which correspond to the ε_{VM} values achieved in rolling (see Fig. 1). From the above measurements, the IPFs corresponding to the RD-TD section and Z-θ section were obtained by making suitable rotations. EBSD for both Ni and Ti deformed samples was carried out by FEGSEM (FEI made Inspect F model) equipped with high-speed HIKARI camera using TSL OIM™ data acquisition and post-processing software (version 7.2). The EBSD scans for the initial state of Ni and Ti were performed with a step size of 1 μm. The EBSD scans were performed with a step size of 50 nm for the Ni samples deformed to the strain of 2.65 while for other deformed samples a step size of 300 nm was used. The grain boundary

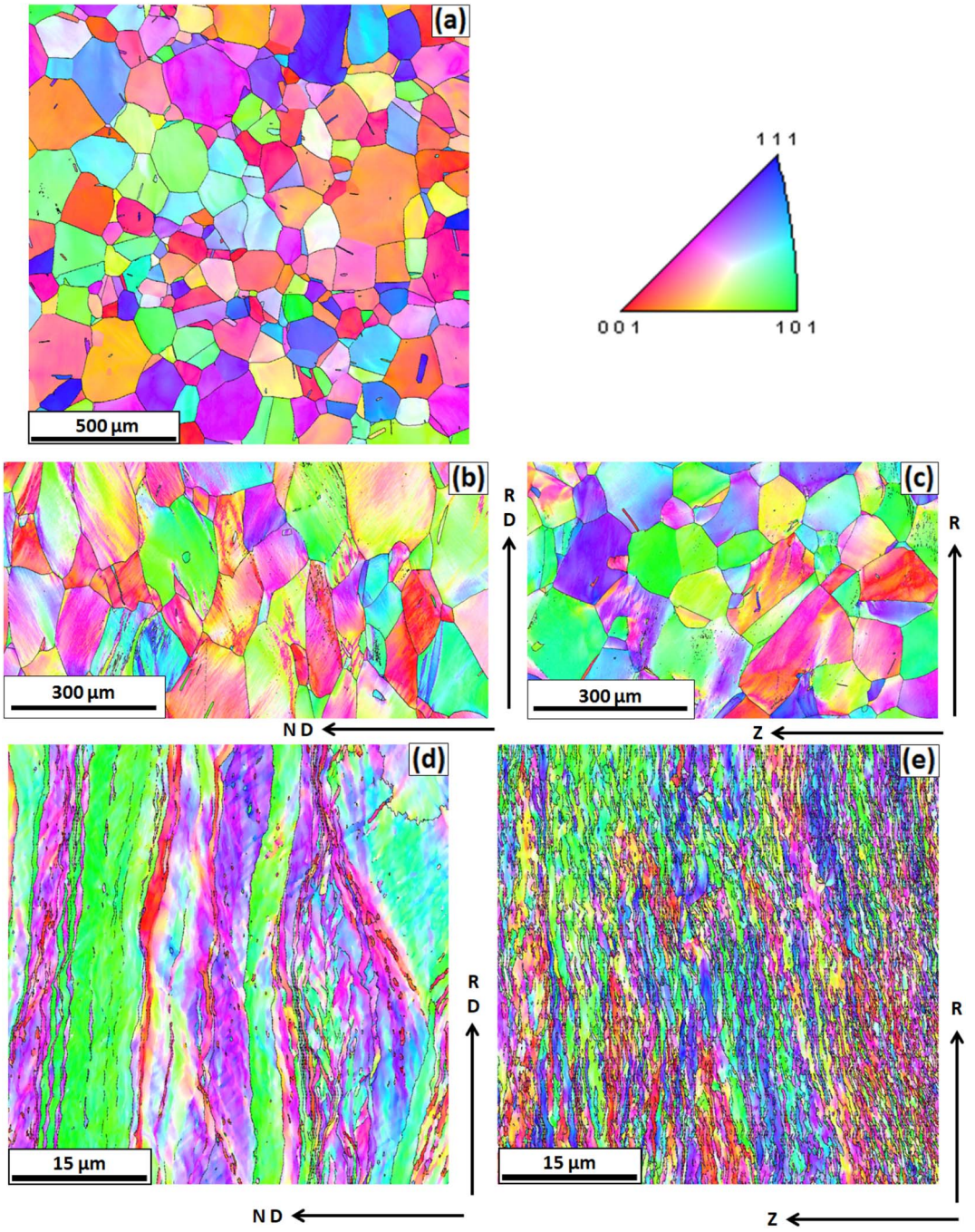

Fig. 2. Inverse pole figures of (a) initial state of Ni sample, EBSD scan performed on section perpendicular to ED. (b) rolled to $\varepsilon_{VM} = 0.5$, (c) torsion deformed to $\varepsilon_{VM} = 0.5$, (d) rolled to $\varepsilon_{VM} = 2.65$ and (e) torsion deformed to $\varepsilon_{VM} = 2.65$. Colour code in rolled and torsion deformed samples correspond to RD-TD section and *Z*-θ section, respectively.

misorientation distribution and the number-averaged grain size (equivalent grain diameter) were determined from the EBSD images. The grains were considered as the regions in the EBSD images bounded by grain boundaries having misorientation higher than 5°.

3. Results

3.1. Microstructure of the Rolled and the Torsion Tested Ni Samples

Fig. 2a–e shows the inverse pole figure maps (IPF) of the initial Ni sample, and the specimens rolled and torsion deformed to $\varepsilon_{VM} = 0.5$ and 2.65. The initial material has a grain size with the average diameter of about 57 µm (standard deviation: 55 µm). In the case of rolling, the grains are elongated along the rolling direction. Most of the grains have their orientation close to {112} and {110}. Orientation gradients within the grains of the rolled and the torsion deformed samples are due to grain subdivision that has occurred during deformation. In the Ni sample rolled to $\varepsilon_{VM} = 0.5$, orientation gradients are observed in all grains and they are elongated along the rolling direction. The development of orientation gradients in rolling can be attributed to the constraint experienced during deformation and thus the grains cannot rotate freely as in the case of torsion. In the rolled Ni samples deformed to $\varepsilon_{VM} = 2.65$, bands of elongated grains parallel to the rolling direction are observed. The microstructure of the torsion deformed sample is more refined compared to the rolled sample. The average grain sizes obtained by EBSD are ~400 and ~330 nm for the Ni samples rolled and torsion tested to the strain of 2.65, respectively.

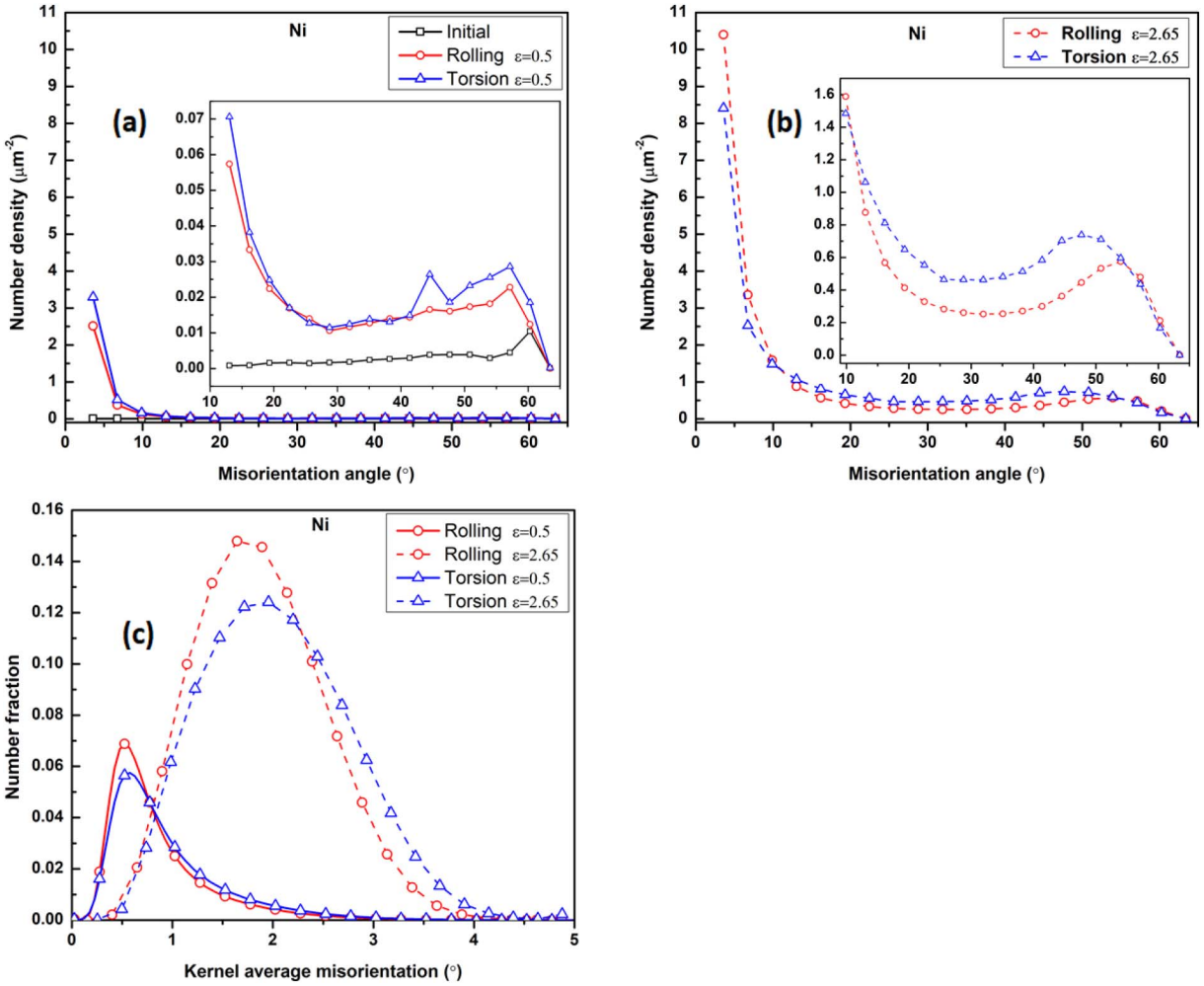

Fig. 3. Misorientation distribution of Ni deformed to (a) ε_{VM} = 0.5, (b) ε_{VM} = 2.65 and (c) kernel average misorientation distribution.

The grain boundary misorientation distributions in the angle range between 3 and 65° for the Ni samples rolled and torsion tested to the equivalent strains of 0.5 and 2.65 are shown in Fig. 3a and b, respectively. For ε_{VM} = 0.5, the torsion tested sample has only marginally higher low angle and high angle grain boundary densities than for the rolled Ni sample. At the same time, in the case of Ni samples deformed to ε_{VM} = 2.65 the low angle grain boundary density (between 3 and 10°) in the rolled sample is higher as compared to the torsion deformed samples, whereas the torsion tested sample has a higher high angle grain boundary (between 10 and 65°) density than the rolled sample. The deformation during torsion is less constrained than in rolling and therefore rotation of grains is easier during torsion deformation. Thus, the higher fraction of high angle grain boundaries in the torsion tested sample deformed to the strain of 2.65 can be attributed to grain subdivision due to slip activity and rotation of subgrains during deformation, resulting in the formation of high angle grain boundaries. The kernel average misorientation (KAM) distribution for the Ni samples deformed to the equivalent strains of 0.5 and 2.65 are shown in Fig. 3c. For the samples deformed to the strain of 2.65, the EBSD step size was smaller (50 nm) than for other specimens (300 nm). Therefore, for the former samples the KAM corresponding to the 6th neighbour was used for the comparison with EBSD scans run with 300 nm step size. For both lower and higher strains, the KAM of the torsion deformed specimens is higher than for the rolled samples.

Fig. 4 shows the CMWP fitting for the Ni sample deformed by torsion for the von Mises equivalent strain of about 2.65. The open circles and the solid line represent the measured and the fitted intensity profiles, respectively. The parameters of the dislocation structure determined from the diffraction patterns for the Ni specimens deformed by rolling and torsion are listed in Table 1. The dislocation density in the torsion tested sample is $\sim 21 \times 10^{14}\ m^{-2}$ which is ~20% higher than in the rolled specimen. The dislocation arrangement parameter, *M*, on the other hand is much larger (nearly 2 times) for the torsion tested

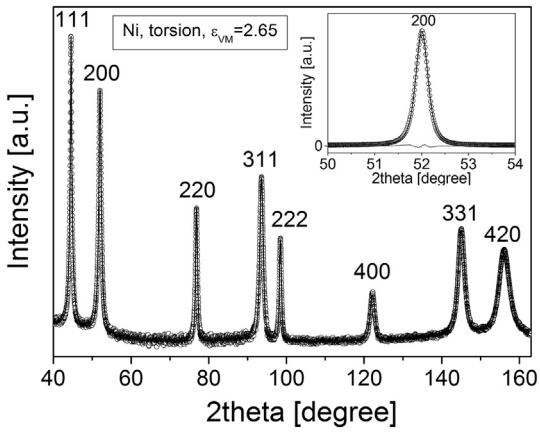

Fig. 4. CMWP fitting for the Ni sample deformed by torsion to the equivalent strain of 2.65. The open circles and the solid line represent the measured and the fitted diffraction patterns, respectively. The intensity is shown in logarithmic scale. The inset illustrates the quality of fitting by showing the difference between the measured and fitted data for reflection 200 which is plotted with linear intensity scale.

Table 1
Parameters of the microstructure determined by XLPA for the rolled and torsion deformed Ni samples. $< x >$: mean crystallite size, ρ: average dislocation density, M: dislocation arrangement parameter. E_{disl}: energy stored in dislocations, d: grain size from EBSD with grain tolerance angle of 5°.

Sample	$< x >$ [nm]	ρ [10^{14} m^{-2}]	M	E_{disl} [10^{6} Jm^{-3}]	d [nm]
Ni, rolling, $\varepsilon_{VM} = 2.65$	46 ± 5	17 ± 2	2.3 ± 0.3	4.0 ± 0.6	400 ± 30
Ni, torsion, $\varepsilon_{VM} = 2.65$	65 ± 7	21 ± 2	4.4 ± 0.5	5.4 ± 0.7	330 ± 25

sample than for the sample deformed by rolling. This difference indicates that the shielding of the strain field of dislocations in the rolled sample is higher than for the torsion-tested material. The higher shielding of the strain field in the rolled sample can be achieved by arranging dislocations into low energy configurations, such as dipoles and low angle grain boundaries for dislocations with opposite and same signs, respectively. This observation is in line with the lower KAM values obtained from the EBSD analysis. The grain sizes determined by EBSD and the crystallite sizes obtained by XLPA are given in Table 1. The difference between the grain and crystallite sizes is due to the hierarchical nature of the microstructures in plastically deformed metals where the grains are subdivided into subgrains and/or dislocation cells which scatter X-rays incoherently [21]. Therefore, the crystallite size (also called as coherently scattering domain size) determined by XLPA corresponds to the size of subgrains and cells. As a consequence, the crystallite size is smaller than the grain size in plastically deformed materials. In EBSD, the grain sizes are determined using a misorientation angle criterion of 5° due to which the subgrains whose misorietation is smaller than 5 ° are not considered in the grain size estimation.

3.2. Microstructure of the Rolled and Torsion Deformed Ti Specimens

The microstructure of the initial, extruded Ti sample is shown in Fig. 5a. The average grain size of this specimen is ~28 μm (the standard deviation is 23 μm). The initial Ti material has a texture in which the hexagonal c-axis is perpendicular to the extrusion direction (denoted by ED) as shown by the 0002 pole figure in Fig. 5b. This texture is typical for extruded hexagonal metallic materials. The microstructures deformed by rolling and torsion to the strains of 0.33 and 0.5 are shown in Fig. 5c–f. The grain sizes obtained from EBSD for the rolled and the torsion deformed Ti samples are listed in Table 2. It can be concluded that both rolling and torsion resulted in a one order of magnitude reduction of the average grain size to about 2–3 μm. The grain sizes for the rolled and torsion tested samples were similar except for the specimen rolled to the strain of 0.5 (Table 2). In the sample rolled to a strain of 0.5, the smaller grain size is caused by the higher twin boundary density as it will be shown later. In our analysis, the twin boundaries were also included in the HAGBs, therefore their formation inside the original grains resulted in a grain refinement for the specimen rolled to the strain of 0.5. The misorientation distributions for the angle range between 5 and 95° in the rolled and torsion tested samples are shown in Fig. 6a. The peaks at the misorientation angles of ~65° and ~85° correspond to the $\{11\bar{2}2\}\langle 11\bar{2}\bar{3}\rangle$ type compressive twins and the $\{10\bar{1}2\}\langle\bar{1}011\rangle$ type tensile twins, respectively [12]. The number densities of twin boundaries in the misorientation distribution are much higher for the sample rolled to the strain of 0.5 than for other samples. This observation is in line with the smaller grain size in this sample as discussed above. The KAM distributions for the Ti samples deformed to the equivalent strains of 0.33 and 0.5 are shown in Fig. 6b. For the strain of 0.33, there is only a slight difference in the average KAM values for the two specimens and the torsion tested sample has only a marginally higher KAM compared to the rolled sample. However, for the strain of 0.5 the average KAM is much higher for the rolled sample.

The IPF map in Fig. 5c shows that in addition to the dislocation slip there is a significant twinning activity during rolling of titanium to the strain of 0.33. In this sample, the tensile twin boundary density is higher than the compression twin boundary density (see Fig. 6a). With increasing the strain from 0.33 to 0.5 during rolling, the twin boundary density considerably increased as shown in Figs. 5e and 6a. This extensive twinning resulted in a grain refinement in the Ti sample rolled to the strain of 0.5 (see Table 2). It is also evident from Fig. 6a that in the initial stage of rolling the tensile twin activity is dominant while with increasing the strain to 0.5 the compression twin boundaries became similarly significant. The considerable increase in low angle boundary (between 3 and 10°) density and orientation colour gradient within the twinned regions in the sample rolled to the strain of 0.5 indicate the occurrence of deformation through slip activity within the newly formed twinned regions (Fig. 5e).

The microstructures of the Ti samples deformed to the strains of about 0.3 and 0.5 were also examined by XLPA. Fig. 7 illustrates the CMWP fitting for the Ti sample deformed by rolling to the von Mises equivalent strain of about 0.5. The open circles and the solid line represent the measured and the fitted intensity profiles, respectively. The parameters of the microstructure determined from the diffraction patterns for the specimens deformed by rolling and torsion for two different equivalent strains are listed in Table 2. It should be noted that similar to the Ni samples, the values of the crystallite size determined by XLPA for the Ti specimens are much smaller than the grain sizes obtained by EBSD. The reason of this difference is the hierarchical nature of the microstructures of the plastically deformed metals as discussed above. The average crystallite sizes in the rolled samples is smaller than that for the torsion tested specimens (see Table 2), indicating more refined subgrain structures in the rolled samples.

For the strain of 0.33, the dislocation density in the rolled sample is ~4.5×10^{14} m^{-2} which is about 50% higher than in the torsion tested specimen. At the same time, the dislocation arrangement parameter, M, for both the torsion tested and the rolled samples is almost the same. With increasing the strain from 0.33 to 0.5, the dislocation density in the rolled Ti increased moderately by about ~17% to ~5.3×10^{14} m^{-2} while there is no change in the arrangement parameter of dislocations (see Table 2). However, for the torsion tested material the increase of the strain from 0.33 to 0.5 resulted in a significant increase (with ~50%) of the dislocation density and a decrease of the value of M, indicating the arrangement of dislocations into low energy configurations (e.g., LAGBs or dipolar walls). For the strain of 0.5, the less clustered dislocation structure in the rolled sample is in line with the much higher average KAM value as compared to the torsion tested specimen.

In hexagonal crystals there are eleven families of slip systems on basal, prismatic and pyramidal planes with three different Burgers vectors [22]. The eleven dislocation slip system families can be classified into three groups based on their Burgers vectors: ($< a >$ type), $b_2 = \frac{1}{3}\langle 0001\rangle$ ($< c >$ type) and $b_3 = \frac{1}{3}\langle\bar{2}113\rangle$ ($< c + a >$ type). The distribution of dislocations in the eleven slip systems can also be estimated from the CMWP evaluation, as described in detail in [23]. Table 3 shows the fractions of dislocations with $< a >$, $< c >$ and $< c + a >$ Burgers vectors. For all samples, the majority of dislocations have $< a >$ and $< c + a >$ Burgers vectors with the fractions of 27–54% and 42–59%, respectively. The contribution of $< c >$ -type dislocations is marginal (less than 14%). Similar to the dislocation density and the dislocation arrangement parameter, the fractions of dislocations did not change with increasing strain for the rolled samples. On the other hand, in the torsion tested materials the fraction of $< c + a >$ dislocations increased with increasing strain. For the

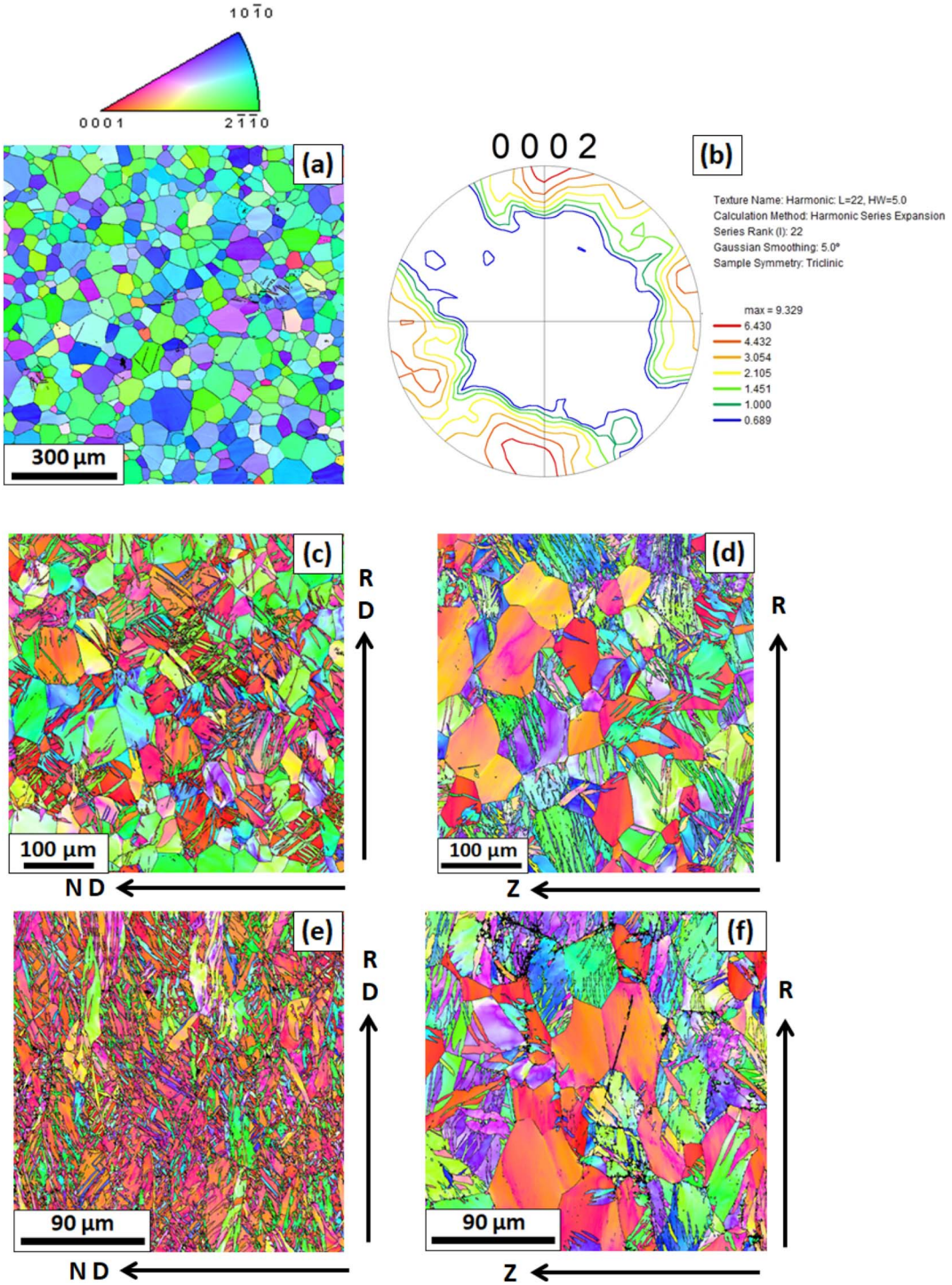

Fig. 5. (a) Inverse pole figure for the initial, extruded Ti sample performed on the section perpendicular to extrusion direction ED. (b) 0002 pole figure determined from the inverse pole figure shown in (a). (c) Inverse pole figure for rolled Ti ($\varepsilon_{VM} = 0.33$), (d) torsion deformed Ti ($\varepsilon_{VM} = 0.33$), (e) rolled Ti ($\varepsilon_{VM} = 0.5$) and (f) torsion deformed Ti ($\varepsilon_{VM} = 0.5$). Colour code in rolled and torsion deformed samples correspond to RD-TD section and Z-θ section, respectively.

Table 2
Parameters of the microstructure determined by XLPA for the rolled and torsion deformed Ti samples. $< x >$: mean crystallite size, ρ: average dislocation density, M: dislocation arrangement parameter. E_{disl}: energy stored in dislocations, d: grain size from EBSD with grain tolerance angle of 5°.

Sample	$< x >$ [nm]	ρ [10^{14} m^{-2}]	M	E_{disl} [10^{6} Jm^{-3}]	d [nm]
Ti, rolling, $\varepsilon_{VM} = 0.33$	40 ± 5	4.5 ± 0.5	4.1 ± 0.5	2.5 ± 0.4	3700 ± 230
Ti, torsion, $\varepsilon_{VM} = 0.33$	71 ± 8	3.1 ± 0.4	4.1 ± 0.4	1.8 ± 0.2	3260 ± 210
Ti, rolling, $\varepsilon_{VM} = 0.5$	25 ± 3	5.3 ± 0.6	4.3 ± 0.5	2.8 ± 0.4	1790 ± 43
Ti, torsion, $\varepsilon_{VM} = 0.5$	68 ± 7	4.6 ± 0.5	2.8 ± 0.3	2.8 ± 0.4	3050 ± 115

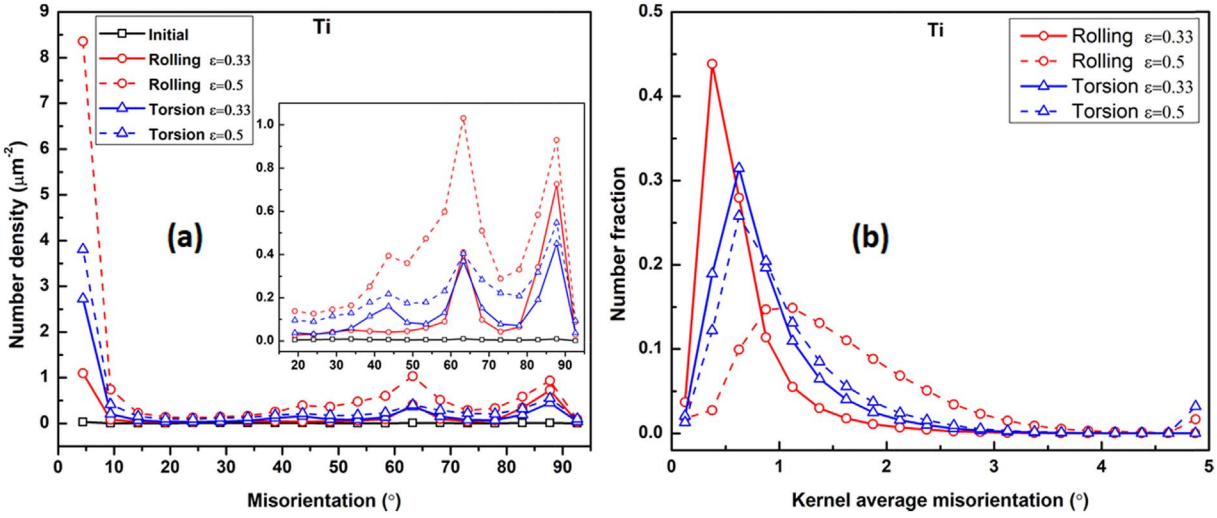

Fig. 6. (a) Misorientation distribution and (b) Kernel average misorientation distribution of Ti deformed to ε_{VM} of 0.33 and 0.5.

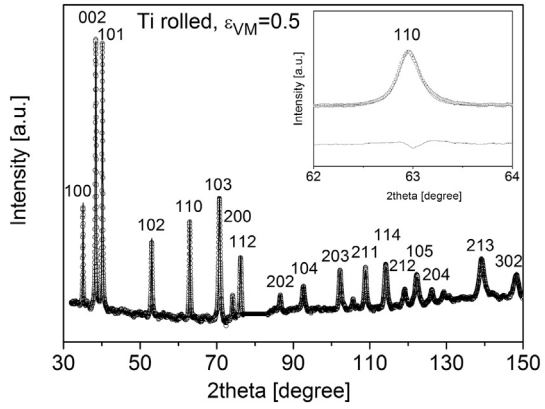

Fig. 7. CMWP fitting for the Ti sample deformed by rolling up to the equivalent strain of 0.5. The open circles and the solid line represent the measured and the fitted diffraction patterns, respectively. The intensity is shown in logarithmic scale. The inset illustrates the quality of fitting by showing the difference between the measured and fitted data for reflection 110 which is plotted with linear intensity scale.

Table 3
The fractions of dislocations with $< a >$, $< c >$ and $< c + a >$ Burgers vectors.

Sample	$< a >$ [%]	$< c >$ [%]	$< c + a >$ [%]
Ti, rolling, ε_{VM} = 0.33	51 ± 6	2 ± 2	47 ± 5
Ti, torsion, ε_{VM} = 0.33	47 ± 5	11 ± 3	42 ± 4
Ti, rolling, ε_{VM} = 0.5	54 ± 6	3 ± 3	43 ± 5
Ti, torsion, ε_{VM} = 0.5	27 ± 4	14 ± 3	59 ± 5

strain of 0.5, the fractions of $< c >$ and $< c + a >$ dislocations are much larger in the torsion tested sample than in the rolled specimen. This indicates a larger contribution of dislocations to the shear in the hexagonal *c*-direction for the torsion tested sample. The smaller activity of $< c >$ and $< c + a >$ dislocations in the rolled sample is compensated by twinning as seen from the misorientation distributions obtained from EBSD (see Fig. 6a).

4. Discussion

4.1. Difference in the Microstructures Obtained by Rolling and Torsion

For the Ni samples deformed to the same high equivalent strain (ε_{VM} = 2.65), the rolled material has a higher grain size with less distorted grain interiors compared to the torsion tested specimen. The smaller lattice strain inside the grains can be attributed to the more clustered dislocation structure as indicated by the smaller value of the dislocation arrangement parameter *M* (Table 1). The deformation during rolling is more constrained and the deformation occurs through multiple slip system activity resulting in generation of dislocations of three or more different Burgers vectors [24,25]. The subgrains formed during the initial stage of deformation undergo very limited rotation in rolling. The formation of stable texture further restricts the rotation of subgrains. As a result of this, the low angle grain boundary fraction is quite significant in rolling. The smaller lattice strain in the rolled samples can be attributed to the nature of slip activity during rolling. In the case of torsion, deformation occurs with slip along a single slip direction, resulting in the generation of dislocations of the same type (i.e., the same Burgers vector) [24,26,27]. Also, the subgrains can rotate freely about the torsion rotation axis. This results in the formation of high angle grain boundaries in torsion and contributes to the larger degree of grain refinement.

In the comparison of the very different microstructures formed in Ti during rolling and torsion to the strain of 0.5, we should consider the texture of the initial, extruded material. In this texture, the c-axis is perpendicular to the extrusion direction. As the torsion axis is parallel to the extrusion direction, large shear stresses operate during torsion in the prismatic and pyramidal lattice planes lying approximately perpendicular to ED. These stresses induce very strong activities of $< c >$ and $< c + a >$ dislocations in the torsion tested specimen. For the rolled Ti samples, the RD-TD plane was perpendicular to ED, therefore in many grains the hexagonal c-axis lies in the rolled sheet. If the friction during rolling is negligible, the maximum shear stresses operate in the planes with the inclination angle of 45° to the rolled sheet (similar to uniaxial compression). In the presence of friction forces, the inclination angle deviates slightly from the value obtained for the friction-free case. Nevertheless, the highest shear stresses do not act parallel to the majority of the prismatic and pyramidal planes during rolling, therefore the activity of $< c >$ and $< c + a >$ dislocations is not so strong when compared to the torsion deformation. As plastic deformation in hexagonal c-direction can be accommodated either by slip of $< c >$ / $< c + a >$ dislocations or twinning, the decrease of the slip activity of $< c >$ / $< c + a >$ dislocations is accompanied by an increased contribution of twinning to plasticity. In addition, during rolling the sheet was compressed in direction ED, i.e., perpendicular to the c-axis which resulted in tensile stresses in the crystallographic direction ⟨0002⟩. This stress state is beneficial for $\{10\bar{1}2\}\langle\bar{1}011\rangle$ type tensile twinning [15]. The occurrence of this twin mode results in a change of c-axis orientation by 85°, i.e., the c-axis became parallel to the compression direction during the next steps of rolling. Therefore, in

the subsequent steps of rolling applied for the achievement of the high strain of 0.5, $\{11\bar{2}2\}\langle 11\bar{2}3\rangle$ type compressive twins were formed in the formerly twinned regions. This process is referred to as double twinning and explains the increased fraction of compressive twins for rolling at high strains [15]. It is noted that Salem et al. [28] have also reported lower twin density for Ti deformed by simple shear when compared with uniaxial compression. In the present case, during torsion (which resembles to simple shear deformation) the propensity of twinning is less compared to rolling in which compressive stresses were developed.

4.2. Estimation of Stored Energies for the Rolled and the Torsion Tested Ni and Ti

In the recrystallization behaviour of plastically deformed materials, the stored energy has a crucial role since it acts as a driving force for the nucleation and growth of new, defect-free grains. It may be noted that the stored energy in deformed materials has contributions predominantly from geometrically necessary dislocations (GNDs) and statistically stored dislocations (SSDs). Different techniques viz. differential scanning calorimetry (DSC), X-ray diffraction, neutron diffraction, EBSD and transmission electron microscopy (TEM) are employed to estimate the stored energy of deformation [29]. The stored energies obtained from each of these techniques were reported to be significantly different [30]. The differences in stored energy are attributed to the differences in the volume as well as whether contributions from both GNDs and SSDs are being obtained or not. The stored energy values obtained from DSC is always reported to be higher compared to other techniques [30]. EBSD and TEM based techniques are widely used for localized stored energy estimation. In the present study, stored energies are estimated from XLPA and EBSD techniques. Contributions from both GNDs and SSDs are accounted for in the stored energy estimation based on XLPA technique and also the data corresponds to the bulk due to large interaction volume. Due to the limitations of the angular resolution of EBSD technique, the stored energy contributions from SSDs cannot be estimated. This is because SSDs do not cause misorientations measurable by EBSD. However, the EBSD based technique is ideal for measuring spatial variation of local stored energy and statistically significant data can be obtained from large areas [29].

The energy stored in the dislocation structure (E_{disl}) for a unit volume in Ni can be determined from the dislocation density using the following formula:

$$E_{disl} = AGb^2\rho \ln\frac{R_e}{b}, \tag{3}$$

where G is the shear modulus (8.2×10^{10} Pa), b is the magnitude of the Burgers vector (0.25 nm), ρ is the dislocation density, R_e is the outer cut-off radius of dislocations (also obtained by XLPA as $M\rho^{-1/2}$) and A stands for the factor depending on the edge/screw character of dislocations. The value of A equals to $(4\pi)^{-1}$ and $(4\pi(1\text{-}\nu))^{-1}$ for screw and edge dislocations, respectively, where ν is the Poisson's ratio (0.3 was taken). The values of R_e were 55 and 98 nm for the rolled and the torsion-tested Ni specimens, respectively. The parameter q determined from XLPA describes the edge/screw character of dislocations. The theoretically calculated values of q for pure edge and screw dislocations in Ni are 1.38 and 2.21, respectively. In the case of mixed dislocations, the value of A can be obtained from the experimentally determined q using a simple rule of mixture:

$$A = \frac{q-1.38}{0.83}\frac{1}{4\pi} + \frac{2.21-q}{0.83}\frac{1}{4\pi(1-\nu)}. \tag{4}$$

For both the rolled and the torsion-tested samples investigated in this study, the value of q was 2.1. The energies stored in dislocations for the rolled and the torsion-tested samples were calculated from Eqs. (3) and (4) and listed in Table 1. In accordance with the slightly larger dislocation density and the less shielded dislocation structure, the stored energy for the torsion-tested specimen is $\sim 5.4 \times 10^6$ Jm^{-3} which is about 35% larger than for the rolled sample, i.e., the thermodynamic driving force for recrystallization is higher for the torsion tested material. The difference in the stored energies obtained for the rolled and the torsion deformed samples can be attributed to the less clustered dislocation structure in the latter specimen which is indicated by the higher value of the dislocation arrangement parameter, M, determined by XLPA (see Table 1).

The energy stored in a unit volume for dislocations in Ti (E_{disl}) can be determined from the dislocation density using the following formula:

$$E_{disl} = G\rho \sum_{i=1}^{11} A_i f_i b_i^2 \ln\left(\frac{R_e}{b_i}\right), \tag{5}$$

where G is the shear modulus (44 GPa), ρ is the dislocation density, R_e is the outer cut-off radius of dislocations (also obtained by XLPA), A_i stands for the factor depending on the edge/screw character of dislocations, b_i is the magnitude of Burgers vector for the *ith* dislocation slip system. The value of A_i equals $(4\pi)^{-1}$ and $(4\pi(1\text{-}\nu))^{-1}$ for screw and edge dislocations, respectively, where ν is the Poisson's ratio (0.3 was taken). The energies stored in dislocations for the rolled and the torsion-tested samples were calculated from Eq. (5) and listed in Table 2. The stored energy for the rolled specimen at the strain of 0.33 is considerably larger than for the torsion-tested sample, i.e., the thermodynamic driving force for recrystallization is higher for the rolled titanium. At the same time, at the strain of 0.5 the energy stored in dislocations for the torsion tested sample is not different from the value obtained for the rolled specimen. At first sight, it is a surprising result as the arrangement parameter of dislocations is smaller for the sample torsion tested to the strain of 0.5. However, the fractions of $< c >$ and $< c + a >$ dislocations are much larger for the torsion tested sample than for the rolled specimen and these dislocations have higher energy due to their larger Burgers vectors, compared to $< a >$ dislocations. It seems that the latter effect compensates the former one, resulting in similar stored energies in the specimens rolled and torsion tested to the strain of 0.5.

From the average KAM value, the stored energy was estimated following the procedure outlined in [31] using the relation,

$$E = \frac{\alpha\theta Gb}{2d}, \tag{6}$$

where α is a constant which depends on the geometry of the dislocation arrangement and is taken as 3, θ is the average KAM in radians, G is the shear modulus, b is the average Burgers vector and d is the step size (300 nm used in the present study).

The stored energy estimated on the basis of EBSD is given in Table 4. For Ni deformed to the equivalent strain of 0.5, there is only a negligible difference between the energies stored in the torsion tested and the rolled specimens. At the same time, for the strain 2.65, the torsion deformed samples have higher stored energy than for the rolled Ni samples. The difference in the stored energy between the rolled and the torsion deformed samples could be due to the difference in slip activity during deformation.

For the rolled and the torsion tested Ti, the stored energies are given

Table 4
Stored energy obtained from EBSD.

Sample	Stored energy from EBSD (MJ m^{-3})
Ni, rolling, ε_{VM} = 0.5	1.5 ± 0.12
Ni, torsion, ε_{VM} = 0.5	1.7 ± 0.07
Ni, rolling, ε_{VM} = 2.65	4.5 ± 0.13
Ni, torsion, ε_{VM} = 2.65	5.7 ± 0.25
Ti, rolling, ε_{VM} = 0.33	1.0 ± 0.1
Ti, torsion, ε_{VM} = 0.33	1.4 ± 0.2
Ti, rolling, ε_{VM} = 0.5	2.4 ± 0.3
Ti, torsion, ε_{VM} = 0.5	2.0 ± 0.2

in Table 4. The stored energies determined by EBSD for the samples rolled and torsion tested for $\varepsilon_{VM} = 0.33$ were 1.0 ± 0.1 and 1.4 ± 0.2 MJ/m^3, respectively. For $\varepsilon_{VM} = 0.5$, the values of 2.4 ± 0.3 and 2.0 ± 0.2 MJ/m^3 were obtained by EBSD for the stored energies in the rolled and the torsion tested specimens, respectively. In this calculation, the Burgers vector in Eq. (6) was calculated as the average of the Burgers vectors for $< a >$, $< c >$ and $< c + a >$ dislocations weigthed by their fractions given in Table 3. The difference in the stored energy between the rolled and the torsion deformed samples is attributed to the differences in slip and twinning activities during rolling and torsion deformation.

The deviation of the EBSD stored energy from the value determined by XLPA can be explained by (i) the much larger volume studied by XLPA (better statistics of the obtained values) and (ii) the large EBSD step size (300 nm) compared to the average spacing of dislocations (about 50 nm calculated as the reciprocal of the square root of the dislocation density). Due to the latter effect, it is possible that not all misorientations caused by the dislocation structure are determined by EBSD, therefore the stored energy is smaller than that obtained by XLPA. In addition, the statistically stored dislocations do not cause misorientations measurable by KAM, therefore this method can yield only a part of the stored energy.

It should be noted that the stored energy calculated in this study is related only to dislocations. In plastically deformed metals, other lattice defects, such as excess vacancies and grain boundaries also contribute to the stored energy. These contributions were not determined in this work as the concentration of vacancies and the specific grain boundary energy in the present rolled and torsion tested Ni and Ti samples are unknown. However, former studies have shown that dislocations give the major part of the stored energy in plastically strained metallic materials which was unambiguously determined in this study. From the systematic study performed in the present work, it is very clear that the mode of deformation through which material undergoes deformation has significant effect on the defect structure and the stored energy. In addition, in the case of titanium the contributions of dislocation slip and twinning to plasticity are also influenced by the method of plastic straining. Thus, the mode of deformation is expected to have a significant effect on the recrystallization behaviour which will be investigated in another study.

5. Conclusions

Ni and Ti samples deformed through rolling and torsion to same equivalent strains were characterized by XLPA and EBSD. The following conclusions can be drawn from the results:

- The rolled Ni sample has larger grains with less distorted grain interiors than in the torsion tested specimen deformed to the same high equivalent strain of 2.65. The smaller lattice distortion inside the grains can be attributed to the more clustered dislocation structure as indicated by the smaller value of the dislocation arrangement parameter determined by XLPA.
- The stored energy in the samples deformed by torsion is larger than the value obtained for the rolled Ni samples. The higher stored energy for the torsion tested specimens can be explained by the larger intragranular strains and the less clustered dislocation structure as indicated by the KAM obtained from EBSD and XLPA, respectively.
- In the case of the deformed Ti samples, in addition to dislocation slip, twinning had a significant contribution to plasticity. In both rolled and torsion tested samples, $\{11\bar{2}2\}\langle 11\bar{2}3\rangle$ type compressive twins and $\{10\bar{1}2\}\langle\bar{1}011\rangle$ type tensile twins were detected. Due to the texture of the initial extruded material, the occurrence of twinning strongly depended on the mode of deformation. During rolling, the compressive stress acting perpendicular to the hexagonal c-axis yielded the activation of tensile twins. As this twinning mode results in a rotation of the c-axis by 85°, at higher strains compressive twins were also formed. The large twinning activity in the sample rolled to the strain of 0.5 yielded greater grain refinement compared to other specimens. In the torsion tested samples, the texture led to an easier activation of the glide of $< c >$ and $< c + a >$ dislocations by the shear stresses. Therefore, the contribution of twinning to deformation is lower for the specimen torsion tested for the strain of 0.5 than for the rolled sample.
- Despite the various microstructures in the rolled and torsion tested Ti samples, large differences in the stored energies estimated by XLPA were not observed. For instance, in the sample torsion tested for the strain of 0.5 the higher average Burgers vector due to the larger fractions of $< c > / < c + a >$ dislocations is compensated by the more clustered arrangement of dislocations, thereby resulting in a similar stored energy when compared to the rolled specimen.

Acknowledgements

The authors thank Prof. S. Suwas for providing the samples used in this study. CNA and VSS thank the Department of Science and Technology, Government of India for the financial support through a research grant (SB/S3/ME/0019/2014). GK and JG thank the Hungarian Scientific Research Fund, OTKA, for the financial support through a research grant no. K-109021.

References

[1] F.J. Humphreys, M. Hatherly, Recrystallization and Related Annealing Phenomena, Second ed., Elsevier, Oxford, 2004.
[2] R.D. Doherty, D.A. Hughes, F.J. Humphreys, J.J. Jonas, D.J. Jensen, M.E. Kassner, W.E. King, T.R. McNelley, H.J. McQueen, A.D. Rollett, Current issues in recrystallization: a review, Mater. Sci. Eng. A 238 (1997) 219–274, http://dx.doi.org/10.1016/S0921-5093(97)00424-3.
[3] L.J. Barto, R.L. Ebert, Deformation stress state effects on the recrystallization kinetics of molybdenum, Metall. Trans. 6 (1971) 1643–1649, http://dx.doi.org/10.1007/BF02913888.
[4] D.T. McDonald, P.S. Bate, W.B. Hutchinson, Effect of strain path change on recrystallisation in copper, Mater. Sci. Technol. 21 (2005) 693–700, http://dx.doi.org/10.1179/174328405X43171.
[5] J.R. Cowan, R.L. Higginson, W.B. Hutchinson, P.S. Bate, Recrystallisation following non-proportional straining in aluminium, Mater. Sci. Technol. 11 (1995) 1104–1109, http://dx.doi.org/10.1179/mst.1995.11.11.1104.
[6] J.Y. Kang, B. Bacroix, H. Réglé, K.H. Oh, H.C. Lee, Effect of deformation mode and grain orientation on misorientation development in a body-centered cubic steel, Acta Mater. 55 (2007) 4935–4946, http://dx.doi.org/10.1016/j.actamat.2007.05.014.
[7] S. Raveendra, A.K. Kanjarla, H. Paranjape, S.K. Mishra, S. Mishra, L. Delannay, I. Samajdar, P. Van Houtte, Strain mode dependence of deformation texture developments: microstructural origin, Metall. Mater. Trans. A. 42 (2011) 2113–2124, http://dx.doi.org/10.1007/s11661-010-0580-0.
[8] C.N. Athreya, S. Suwas, V.S. Sarma, Influence of mode of deformation on microstructural heterogeneities in Ni subjected to large strain deformation, Philos. Mag. Lett. 95 (2015) 441–449, http://dx.doi.org/10.1080/09500839.2015.1085129.
[9] C.N. Athreya, A. Mukilventhan, S. Suwas, S. Vedantam, V. S. Sarma, Influence of the Mode of Deformation on Recrystallization Kinetics in Nickel Through Experiments, Theory, and Phase Field Model, Philos. Mag., http://dx.doi.org/10.1080/14786435.2017.1370146
[10] S.K. Sahoo, R.K. Sabat, S. Sahni, S. Suwas, Texture and microstructure evolution of commercially pure titanium during hot rolling: role of strain-paths, Mater. Des. 91 (2016) 58–71, http://dx.doi.org/10.1016/j.matdes.2015.11.073.
[11] S. Sinha, A. Ghosh, N.P. Gurao, Effect of initial orientation on the tensile properties of commercially pure titanium, Philos. Mag. 96 (2016) 1485–1508, http://dx.doi.org/10.1080/14786435.2016.1165873.
[12] X. Li, Y.L. Duan, G.F. Xu, X.Y. Peng, C. Dai, L.G. Zhang, Z. Li, EBSD characterization of twinning in cold-rolled CP-Ti, Mater. Charact. 84 (2013) 41–47, http://dx.doi.org/10.1016/j.matchar.2013.07.008.
[13] S.K. Sahoo, R.K. Sabat, B.D. Bishoyi, A.G.S. Anjani, S. Suwas, Effect of strain-paths on mechanical properties of hot rolled commercially pure titanium, Mater. Lett. 180 (2016) 166–169, http://dx.doi.org/10.1016/j.matlet.2016.05.162.
[14] S. Sinha, A. Pukenas, A. Ghosh, A. Singh, W. Skrotzki, N.P. Gurao, Effect of initial orientation on twinning in commercially pure titanium, Philos. Mag. 97 (2017) 775–797, http://dx.doi.org/10.1080/14786435.2017.1279364.
[15] J.W. Won, C.H. Park, S.-G. Hong, C.S. Lee, Deformation anisotropy and associated mechanisms in rolling textured high purity titanium, J. Alloys Compd. 651 (2015) 245–254, http://dx.doi.org/10.1016/j.jallcom.2015.08.075.
[16] S. Panda, S.K. Sahoo, A. Dash, M. Bagwan, G. Kumar, S.C. Mishra, S. Suwas, Orientation dependent mechanical properties of commercially pure (cp) titanium, Mater. Charact. 98 (2014) 93–101, http://dx.doi.org/10.1016/j.matchar.2014.10.011.

[17] A. Ghosh, A. Singh, N.P. Gurao, Effect of rolling mode and annealing temperature on microstructure and texture of commercially pure-titanium, Mater. Charact. 125 (2017) 83–93, http://dx.doi.org/10.1016/j.matchar.2017.01.022.
[18] J.W. Won, T. Lee, S.-G. Hong, Y. Lee, J.H. Lee, C.S. Lee, Role of deformation twins in static recrystallization kinetics of high-purity alpha titanium, Met. Mater. Int. 22 (2016) 1041–1048, http://dx.doi.org/10.1007/s12540-016-6369-y.
[19] B. Beausir, L.S. Tóth, F. Qods, K.W. Neale, Texture and mechanical behavior of magnesium during free-end torsion, J. Eng. Mater. Technol. 131 (011108) (2009) 1–15, http://dx.doi.org/10.1115/1.3030973.
[20] G. Ribárik, J. Gubicza, T. Ungár, Correlation between strength and microstructure of ball-milled Al–Mg alloys determined by X-ray diffraction, Mater. Sci. Eng. A 387–389 (2004) 343–347, http://dx.doi.org/10.1016/j.msea.2004.01.089.
[21] T. Ungár, G. Tichy, J. Gubicza, R.J. Hellmig, Correlation between subgrains and coherently scattering domains, Powder Diffract. 20 (2005) 366–375, http://dx.doi.org/10.1154/1.2135313.
[22] K. Máthis, K. Nyilas, A. Axt, I. Dragomir-Cernatescu, T. Ungár, P. Lukáč, The evolution of non-basal dislocations as a function of deformation temperature in pure magnesium determined by X-ray diffraction, Acta Mater. 52 (2004) 2889–2894, http://dx.doi.org/10.1016/j.actamat.2004.02.034.
[23] J. Gubicza, X-ray Line profile analysis in materials science, IGI Global (2014), http://dx.doi.org/10.4018/978-1-4666-5852-3.
[24] T. Ungár, L.S. Tóth, J. Illy, I. Kovács, Dislocation structure and work hardening in polycrystalline ofhc copper rods deformed by torsion and tension, Acta Metall. 34 (1986) 1257–1267, http://dx.doi.org/10.1016/0001-6160(86)90012-X.
[25] J. Weertman, S.S. Hecker, Theory for saturation stress difference in torsion versus other types of deformation at low temperatures, Mech. Mater. 2 (1983) 89–101, http://dx.doi.org/10.1016/0167-6636(83)90029-7.
[26] C. Tome, G.R. Canova, U.F. Kocks, N. Christodoulou, J.J. Jonas, The relation between macroscopic and microscopic strain hardening in F.C.C. polycrystals, Acta Metall. 32 (1984) 1637–1653, http://dx.doi.org/10.1016/0001-6160(84)90222-0.
[27] G. Canova, S. Shrivastava, J. Jonas, C. G'Sell, The use of torsion testing to assess material formability, in: J. Newby, B. Niemeier (Eds.), Formability of Metallic Materials—2000 A.D., STP28395S, ASTM International, West Conshohocken, PA, 1982, pp. 189–210 (Doi: 10.1520/STP28395S).
[28] A.A. Salem, S.R. Kalidindi, R.D. Doherty, Strain hardening of titanium: role of deformation twinning, Acta Mater. 51 (2003) 4225–4237, http://dx.doi.org/10.1016/S1359-6454(03)00239-8.
[29] A. Godfrey, O.V. Mishin, T. Yu, Characterization and influence of deformation microstructure heterogeneity on recrystallization, IOP Conf. Ser. Mater. Sci. Eng. 89 (2015) 12003, http://dx.doi.org/10.1088/1757-899X/89/1/012003.
[30] T. Knudsen, W.Q. Cao, A. Godfrey, Q. Liu, N. Hansen, Stored energy in nickel cold rolled to large strains, measured by calorimetry and evaluated from the microstructure, Metall. Mater. Trans. A. 39 (2008) 430–440, http://dx.doi.org/10.1007/s11661-007-9421-1.
[31] Y. Takayama, J.A. Szpunar, Stored energy and Taylor factor relation in an Al-Mg-Mn alloy sheet worked by continuous cyclic bending, Mater. Trans. 45 (2004) 2316–2325, http://dx.doi.org/10.2320/matertrans.45.2316.